Converting conventional electron accelerators to high peak brilliance Compton light sources

I. V. Pogorelsky,[1,*] M. Polyanskiy,[1] and T. Shaftan[2]

[1]*Accelerator Test Facility, Brookhaven National Laboratory, building 820M, Upton, New York 11973, USA*

[2]*NSLS-II, Brookhaven National Laboratory, building 744, Upton, New York 11973, USA*

(Received 11 August 2020; accepted 26 October 2020; published 4 December 2020)

Several proposals have been put forward for converting electron accelerators to inverse Compton scattering (ICS) gamma sources. Typical approaches suggest combining near-IR solid-state lasers operating continuously at a multimegahertz repetition rate with e-beams when setting their interaction point inside a field-enhancement, Fabry-Perot optical cavity. We introduce here an alternative method of pairing particle accelerator beams with trains of long-wave-infrared, $\lambda_L \approx 9$–11 μm pulses from a picosecond CO_2 laser of a novel architecture operating in a repetitive pulse-burst mode. Because of a considerable increase in the laser energy per pulse, combined with an order-of-magnitude higher number of laser photons per joule of laser energy, our approach allows us to increase the ICS *peak* flux and brilliance by 4 orders of magnitude compared to previous proposals while maintaining high (10^{11}–10^{12} ph/s) *average* flux. This outcome is supported by the examples of the DAΦNE and CBETA accelerator facilities, where 10^{20}–10^{21} ph/$(s \cdot mm^2 \cdot mrad^2 \cdot 0.1\%BW)$ *peak* brilliances at 50–1000 keV photon energy range can be achieved and is comparable or exceeds the capabilities of contemporary synchrotron light sources at hard x rays. Such high-brightness ICS sources will find applications in pump-probe and other ultrafast studies that require building up meaningful datasets on a single x-ray pulse.

DOI: 10.1103/PhysRevAccelBeams.23.120702

I. INTRODUCTION

X-ray and gamma sources based on Thomson or inverse Compton scattering (ICS) from relativistic electron beams colliding with laser pulses promise to bridge a gap in performance and cost between conventional x-ray tubes and synchrotron light sources (SLSs). For an ICS, a laser can be viewed as a virtual undulator that retains the fundamental virtues of synchrotron radiation, with directionality and monochromaticity among them. Simultaneously, ICS sources offer new capabilities, including the opportunity to move further into hard x-ray and gamma spectral ranges not covered by SLSs. This is possible because the laser wavelength is orders of magnitude shorter compared to the period of a conventional magnetic wiggler array, resulting in a corresponding increase in the frequency of induced relativistic electron oscillations. At the same time, much less energetic electrons are needed for ICS to attain the x-ray range covered by SLSs, thus promising a relative compactness and affordability of ICS sources.

Starting with proof-of-principle demonstrations [1], a concept of dedicated ICS sources is presently being materialized in a working commercial *Lyncean* compact light source [2] operating at soft x rays and in gamma sources under construction, such as the High Energy Accelerator Research Organization (KEK) [3] and Extreme Light Infrastructure Nuclear Physics (ELI-NP) [4]. At the same time, several proposals have been put forward to convert existing or newly constructed electron accelerators to high-power ICS sources [5,6].

Most of those ICS projects are based on combining electron beams with pulses from mode-locked, near-infrared (NIR), $\lambda_L \approx 0.8$–1 μm solid-state lasers. Such lasers can operate at a multimegahertz repetition rate matched to rf e-beam sources, such as a synchrotron and a superconducting energy recovery linac (SERL).

Although mode-locked quasi-cw lasers have a relatively low average power on the order of 100 W, their ability to drive an intense ICS can be enhanced by orders of magnitude via stocking laser pulses inside a high-finesse Fabry-Perot cavity. Tuned in resonance with the laser repetition rate, such a field-enhancement cavity (FEC) accumulates multikilowatts of average laser power spread between short picosecond pulses [7]. Synchronized with counterpropagating

*igor@bnl.gov

electron bunches produced by contemporary high-current accelerators, such laser beams might allow the achievement of $\sim 10^{12}$ ph/s average x-ray fluxes, which are a million times stronger than those achieved with x-ray tubes. This makes ICS sources potent for many applications covered by SLSs, such as providing penetrating radiation for structural studies of materials and biological objects, typically in a new spectral range shifted toward harder x rays.

At the same time, a dual-wavelength combination (laser plus x rays) available with pulsed ICS sources invites their use for pump-probe studies. To accomplish this task, intense x-ray flushes are desirable in order to create meaningful datasets from a single pulse. However, currently limited by the 0.1–1 mJ energy per laser pulse circulating inside an FEC, single-shot x-ray yields from such ICS sources do not exceed thousands of photons per pulse, which is usually below the requirements for pump-probe studies. Cranking up the number of radiated x rays per pulse at a given accelerator current would require a much higher number of laser photons per pulse compared with present NIR FEC technical capabilities.

To address this problem, we propose here an approach based on state-of-the-art short-pulse CO_2 lasers. Conventional atmospheric-pressure CO_2 lasers are not well suited for a quasi-cw, mode-locked regime due to the narrow spectral bandwidth of the active medium [8]. Instead, our proposed concept is based on high-pressure CO_2 laser amplifiers that can produce powerful picosecond pulses [9].

Let us address the merits of the *pulsed* CO_2 laser approach compared to an FEC coupled to a *quasi-cw* mode-locked solid-state laser. What are we gaining and losing from changing the laser driver?

Admittedly, NIR lasers provide easier access to the gamma region compared to CO_2 lasers, which operate at 9–11 μm wavelengths belonging to the long-wave-infrared (LWIR) spectral domain. However, the resulting shift of the ICS output toward a softer x-ray area where the major community of synchrotron radiation users is currently active has its own compelling merits.

The joule-class pulsed CO_2 lasers can deliver high concentrations of laser photons in the laser–e-beam interaction region to produce instantaneous picosecond x-ray fluxes that exceed those attained with NIR-FEC-based ICS sources by several orders of magnitude. This makes CO_2 laser-based ICS sources better positioned for studying dynamic processes at the temporal and energy scales of phase transitions, chemical reactions, and molecular interactions.

Commercially available small-aperture (up to 22 mm) high-pressure CO_2 lasers can operate at a repetition rate of up to 300 Hz [10], and an interelectrode distance of $\sim$50 mm can be achieved with the present state of high-voltage pulse-forming network technology [11]. Combined with the novel approach of multiplying the repetition rate in the pulse-burst mode, which we propose here, this can bring us up to an effective repetition rate of >10 kHz. This is still by orders of magnitude below the multimegahertz repetition rate of rf accelerators and mode-locked solid-state lasers paired to them. However, a much higher pulsed energy attainable with high-pressure CO_2 lasers, coupled with a higher photon number per unit of the laser energy, allows us to reach the same average x-ray photon intensity as an NIR FEC approach despite the difference in the repetition rate.

Eventually, the choice of an x-ray or gamma radiation source for any given application is based on maximizing the number of usable photons delivered within a data acquisition period and the acceptance phase space of a detector system used for that application or experiment. Facing a diversity of potential requirements for future ICS applications, we offer here a comprehensive performance characterization for different kinds of emerging ICS sources based on concrete examples of circular accelerators, including DAΦNE (synchrotron) and CBETA (SERL) paired to either an NIR solid-state laser or an LWIR CO_2 gas laser.

II. ESSENTIAL EXPRESSIONS

A. ICS performance characteristics

We compile here analytical expressions for ICS parameters used in our comparative analysis.

Passing the laser focus, relativistic electrons with velocity $v = \beta c$, where c is the speed of light and β is the relativistic factor, scatter laser photons within a narrow-divergence cone of a half-opening angle $\theta_0 = 1/\gamma$, centered along the electron beam propagation, where $\gamma \equiv \frac{1}{\sqrt{1-\beta^2}} = \mathcal{E}_e[\mathrm{MeV}]/0.511$ is the Lorentz factor and $\mathcal{E}_e$ is the electron energy.

The scattered photons emerge Doppler shifted at the wavelength

$$\lambda_\gamma \approx \frac{\lambda_L}{4\gamma^2}[1 + a_0^2 + \gamma^2\theta^2 + \phi^2/4], \tag{1}$$

where $a_0 = 0.855 \times 10^{-9}\lambda_L\ \mu\mathrm{m}\sqrt{I_L[\mathrm{W\,cm^{-2}}]}$ is the normalized laser vector potential, I_L is the laser intensity, and ϕ is the collision angle. In the case of a counterpropagation geometry, $\phi = 0$, we obtain the shortest wavelength of scattered x rays and the best efficiency of the laser–e-beam interaction. The total number of scattered photons,N_γ, is given by

$$N_\gamma = \sigma_T \frac{N_e N_L}{2\pi(\sigma_e^2 + \sigma_L^2)}, \tag{2}$$

where $\sigma_T = 6.65 \times 10^{-17}\ \mu\mathrm{m}^2$ is the Thomson cross section, N_e is the number of electrons in the bunch, N_L is the number of photons in the laser pulse, and σ_e and σ_L are the rms transverse sizes of the electron and laser beams, respectively.

For ICS sources with the pulse repetition rate f and the individual rms electron bunch length τ_e, the total peak and average fluxes are defined correspondingly as $\mathcal{F}_p = \frac{0.94N_\gamma}{2\sqrt{2\ln 2}\tau_e}$ and $\mathcal{F}_{av} = fN_\gamma$. Here and after, we assume a Gaussian pulse profile. The coefficient 0.94 is the shape factor for a Gaussian pulse, and $2\sqrt{2\ln 2} = 2.36$ corresponds to the transition from rms to FWHM.[1]

Typically, a light source is characterized by the spectral and angular density of the photon flux. In the Thomson backscatter limit, the number of scattered photons in a 0.1% relative bandwidth along the e-beam propagation is given by $N_{0.1\%} = 1.5 \times 10^{-3} N_\gamma$, leading to similar expressions for average and peak spectral fluxes: $\mathcal{F}_{0.1\%av(p)} = 1.5 \times 10^{-3}\mathcal{F}_{av(p)}$.

The brightness (or brilliance) of the scattered photons in the 0.1% bandwidth, defined as a flux per unit solid angle averaged over the cross section of the interaction area, is typically given by $\mathscr{B}_{av(p)} = \frac{\gamma^2\mathcal{F}_{0.1\%av(p)}}{4\pi^2\epsilon_n^2}$, where ϵ_n is the normalized transverse emittance of the electron beam at the interaction point (IP). It is also easy to see the conversion between the average and peak flux and brightness: $\frac{\mathcal{F}_{av}}{\mathcal{F}_p} = \frac{\mathscr{B}_{av}}{\mathscr{B}_p} = f\tau_e 2\sqrt{2\ln 2}/0.94$.

Monochromaticity is an important capability of radiation sources. Several factors can contribute to the spectrum smearing on top of the ideal θ angle dependence factored into Eq. (1). Contributions to the spectral spread may come from both the laser and electron beam.

There are three main contributions to the total x-ray relative energy spread or bandwidth $BW = \frac{\Delta\mathcal{E}_\gamma}{\mathcal{E}_\gamma}$, imposed by the laser [12]: (1) the laser natural bandwidth $\left[\frac{\Delta\mathcal{E}_\gamma}{\mathcal{E}_\gamma}\right]_{\Delta\nu_L} = \frac{\Delta\nu_L}{\nu_L}$ for a transform-limited Gaussian pulse $\tau_L\Delta\nu_L \approx \frac{1}{4\pi}$ and $\left[\frac{\Delta\mathcal{E}_\gamma}{\mathcal{E}_\gamma}\right]_{\Delta\nu_L} \approx \frac{\lambda}{2\tau_L c}$, (2) the laser's natural divergence or diffraction $\left[\frac{\Delta\mathcal{E}_\gamma}{\mathcal{E}_\gamma}\right]_d = \left[\frac{M^2\lambda}{4\pi\sigma_L}\right]^2$, where M^2 is the beam quality factor characterizing the deviation of the laser beam from an ideal Gaussian beam, and (3) "redshift" of the ICS spectral peak upon the laser intensity defined by a_0, $\left[\frac{\Delta\mathcal{E}_\gamma}{\mathcal{E}_\gamma}\right]_{a_0} = \frac{a_0^2/3}{1+a_0^2/2} \approx a_0^2/3$.

In addition, there are two contributions from a nonideal electron beam: (4) normalized electron emittance ϵ_n, $\left[\frac{\Delta\mathcal{E}_\gamma}{\mathcal{E}_\gamma}\right]_\epsilon = \left[\frac{\epsilon_n}{\sigma_e}\right]^2$, and (5) electron beam energy spread $\left[\frac{\Delta\mathcal{E}_\gamma}{\mathcal{E}_\gamma}\right]_{\Delta\gamma} = \frac{2\Delta\gamma}{\gamma}$. Finally, a contribution from a limiting aperture centered on the beam's axis or a finite observation solid angle ("acceptance") with half-opening $\theta_{\max}$ is defined in the following way: (6) $\left[\frac{\Delta\mathcal{E}_\gamma}{\mathcal{E}_\gamma}\right]_\Psi = \Psi^2$, where $\Psi = \gamma\theta_{\max}$. It is practical to choose this aperture close to transmitting all the photons within the total partial bandwidth defined by all the contributions above. Therefore, this contribution is typically set equal to the mean square of all preceding contributions.

The total combined rms bandwidth becomes

$$BW = \frac{\Delta\mathcal{E}_\gamma}{\mathcal{E}_\gamma} = \sqrt{\left[\frac{\Delta\mathcal{E}_\gamma}{\mathcal{E}_\gamma}\right]^2_{\Delta\nu_L} + \left[\frac{\Delta\mathcal{E}_\gamma}{\mathcal{E}_\gamma}\right]^2_d + \left[\frac{\Delta\mathcal{E}_\gamma}{\mathcal{E}_\gamma}\right]^2_{a_0} + \left[\frac{\Delta\mathcal{E}_\gamma}{\mathcal{E}_\gamma}\right]^2_\epsilon + \left[\frac{\Delta\mathcal{E}_\gamma}{\mathcal{E}_\gamma}\right]^2_{\Delta\gamma} + \left[\frac{\Delta\mathcal{E}_\gamma}{\mathcal{E}_\gamma}\right]^2_\Psi}. \tag{3}$$

It is also customary for BW-limited sources to measure their output characteristics within this combined BW. The number of photons in BW and fluxes in BW for small normalized collecting angles $\Psi^2 \ll 1$ are approximately determined by multiplying the corresponding total numbers by Ψ^2. For example, $\mathcal{F}^{bw}_{av,p} \approx \Psi^2 \times \mathcal{F}_{av,p}$.

The spectral density (SPD), defined as a ratio between the photon flux in the BW and the rms value of the bandwidth, can be finally calculated by

$$\mathrm{SPD}_{av,p}\left[\frac{\mathrm{ph}}{\mathrm{s}\cdot\mathrm{eV}}\right] \equiv \frac{\mathcal{F}^{bw}_{av,p}}{\sqrt{2\pi}\Delta\mathcal{E}_\gamma}.$$

The above expressions are routinely used to characterize performance of SLSs. In the next sections, we use those expressions to compare prospective ICS sources based on two different accelerators paired to two kinds of lasers.

B. Choosing LWIR laser parameters

Calculating ICS characteristics by the expressions drawn in the previous section, we will use performance parameters reported for a given accelerator and select parameters for a practically achievable LWIR pulsed laser in a way that optimizes the ICS performance. The performance parameters for ICS sources driven with NIR lasers are adapted (with corrections when deemed necessary) from publications [5,6]. For our complementary concept of a high-peak-brightness ICS source, we propose here a novel design of a high-repetition-rate CO_2 laser system configured to deliver laser beams that allow us to maximize both peak and average ICS x-ray yields at the same time, while also not

[1]The rms pulse duration τ_L and rms beam radius σ_L in the case of a Gaussian temporal- and spatial-intensity distribution are related to FWHM duration τ_{FWHM} and $1/e^2$ radius w traditionally used in laser physics as $\tau_{\mathrm{FWHM}} = 2\sqrt{2\ln 2}\tau_L$ and $w = 2\sigma_L$, respectively.

degrading the BW defined for ICS based on NIR lasers in Refs. [5,6]. Such optimization of laser parameters requires certain restraints that we address here.

In order to maximize the x-ray flux per pulse, we wish to bring as many laser photons in interaction with an electron bunch as possible. This can be accomplished by increasing the laser energy, using a counterpropagation geometry, using the laser focus spot matching the electron beam size, $\sigma_L \approx \sigma_e$, and making the laser pulse short enough so that most of the laser photons efficiently interact with the entire electron bunch within a region where both beams remain focused, which is normally within two effective Rayleigh lengths of the laser focus, $2z_0 = \frac{8\pi\sigma_L^2}{M^2\lambda_L}$. At the same time, when compressing the laser pulse and increasing its intensity, we need to make sure that the laser contributions to the BW do not exceed the targeted number. In particular, we must make sure that tight laser focusing does not boost the laser intensity contribution $[\frac{\Delta\mathcal{E}_\gamma}{\mathcal{E}_\gamma}]_{a_0}$ and the diffraction-limited contribution $[\frac{\Delta\mathcal{E}_\gamma}{\mathcal{E}_\gamma}]_d$ to the BW—with both those numbers being preferably below $[\frac{\Delta\mathcal{E}_\gamma}{\mathcal{E}_\gamma}]_{\Delta\nu_L}$, which is defined by the laser pulse duration. These requirements put certain limits on the laser intensity, pulse duration, and the focus size. For example, assuming the limit for each individual contribution to the BW at 0.25%, we obtain for a CO_2 laser beam (a) $\tau_L \geq 6$ ps or $\tau_{\mathrm{FWHM}} \geq 14$ ps; (b) $\sigma_L \geq 1.6M^2\lambda$, resulting in $\sigma_L \geq 20$ μm for $M^2 \approx 1.2$; and (c) $a_0 \leq 0.08$.

We will follow these rules when selecting CO_2 laser parameters in the next section.

III. LWIR LASER DRIVER FOR ICS SOURCE

A concept for an LWIR laser system for driving a high-brightness ICS source is illustrated in Fig. 1. Many core technical principles of this system are similar to a terawatt-class LWIR laser operated at the BNL Accelerator Test Facility (ATF) [13], currently at a low repetition rate (one shot every 20 s) for multidisciplinary user experiments. The main difference is that the laser system proposed here is designed for a 150 Hz pulse repetition rate based on state-of-the-art offerings by industry [10,11].

A 9.2−μm, bandwidth-limited, picosecond, linear polarized seed laser pulse chosen according to the accelerator

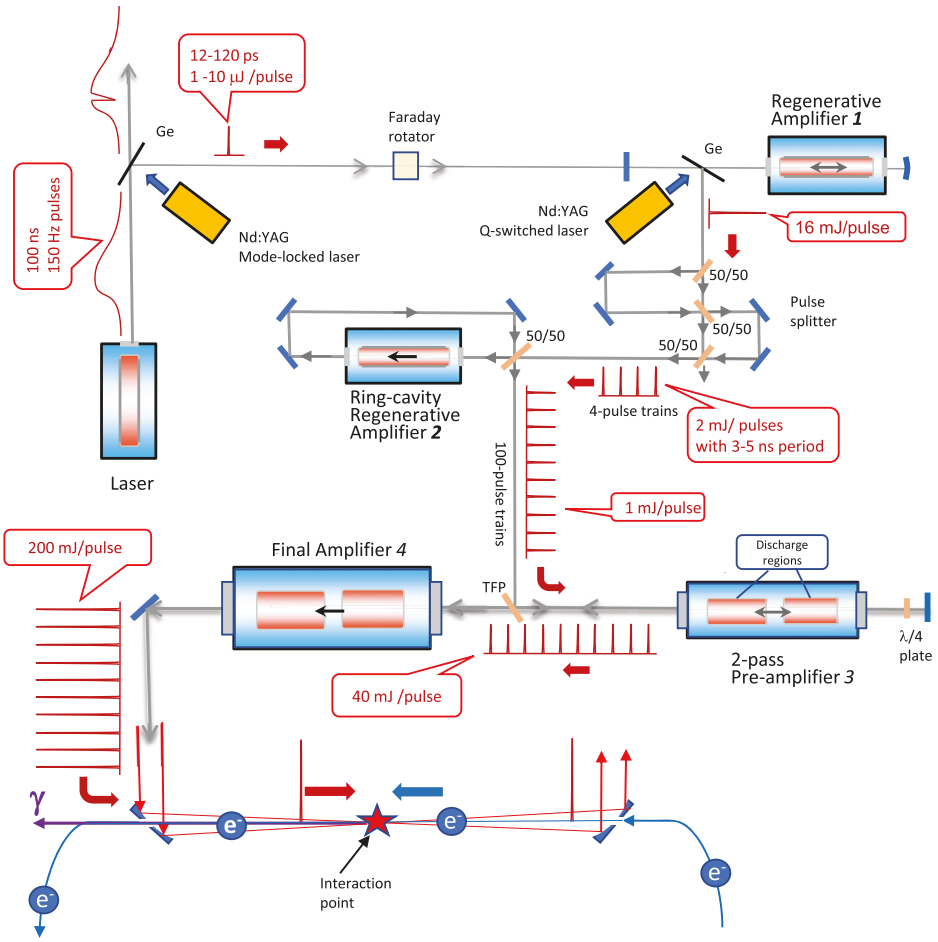

FIG. 1. Principle optical diagram of an LWIR laser system and an ICS interaction region (note that pulse duration is measured at FWHM; TFP stands for thin-film polarizer).

bunch format at an initial energy of ~1 μJ for the case of the 12-ps FWHM pulse or ~10 μJ for the case of the 120-ps FWHM pulse can be sliced from a ~100 ns, ~100 mJ output of a 150-Hz transversely excited atmospheric CO_2 laser oscillator using a semiconductor optical switching method based on a Ge Brewster wafer with the reflection control by an Nd-YAG Q-switched laser [9,14]. An alternative way to generate LWIR picosecond pulses is by using an optical parametric amplifier based on solid-state laser technology [15].

The seed pulse is sent into a regenerative amplifier that amplifies it to 16 mJ. This capability has been demonstrated using a high-pressure, electric discharge, commercial CO_2 amplifier [14]. To avoid the pulse's spectral envelope modulation and narrowing upon amplification that would result in the laser pulse splitting and stretching, the gas-discharge amplifier operates with an isotopic $C^{16,18}O_2$ mixture at 10-atm pressure that ensures a sufficiently broad and smooth gain spectrum [16]. The amplified pulse is extracted from the regenerative cavity using another semiconductor optical switch.

To produce a pulse train with the required time interval between pulses, T_b, we need another regenerative amplifier, ideally with a cavity round-trip period equal to T_b. For the examples below, this period is quite short and requires a compact, few-centimeter-long active amplification module with a high small-signal gain, ~30%/cm, that could be realized based on an ultrahigh-pressure (20–30 atm) CO_2 gas cell optically pumped by laser diodes or solid-state lasers. However, this optical pumping technology is in a developmental stage and has not yet been demonstrated at the required energetics. Therefore, we offer a more conventional approach where all CO_2 gas laser amplifiers in the proposed system are based on a UV-preionized transverse electric discharge. Amplifiers used as active elements at two initial regenerative amplification stages are essentially identical; their technical characteristics are listed in Table I together with other CO_2 laser amplifiers used in the proposed laser system. For the sake of discharge uniformity, CO_2 gas in such an amplifier is strongly diluted with helium, resulting in a reduced small-signal gain, typically ~2%/cm. This requires a much longer active medium, which would not fit into a short optical cavity matched to the T_b period, which varies between 3 and 5 ns in the electron accelerators considered here. Instead, we choose a cavity length that is an exact multiple of the bunch period ($4cT_b$ in our example) and seed it with a short train of four pulses created using a pulse splitter or recombiner. With 50% optical losses on this splitter or recombiner, we will get four 2 mJ pulses.

In the second regenerative amplifier stage, we generate trains of 100-plus pulses at the T_b period at an average energy of ~1 mJ/pulse extracted through a 50% coupling mirror of a ring cavity. A typical gain envelope with the FWHM ≈ 1 μs in such an amplifier allows us to obtain quasiuniform pulse trains within the ~500 ns time interval. These trains are further amplified via a double pass through the third CO_2 laser preamplifier and a single pass through the final laser amplifier. In order to further flatten the pulse train envelope, we assume two independently triggered discharge sections per each of the last two amplifier stages. Optimizing the time delay between discharges in two discharge sections allows us to prolong a quasistationary train section at 200–250 mJ/pulse, extending it over 100 pulses.

Comprehensive modeling of the laser parameters on each stage of the amplifier chain has been performed using the CO2AMP code [17] benchmarked against the ATF laser system, which reaches a total amplification that is 100 times higher than the system proposed here [18]. A simulated pulse train is shown in Fig. 2 for the case of $T_b = 5$ ns and $\tau_L \approx 5$ ps, which are the parameters close to the examples considered in Sec. IV.

A water-cooled, metallic, off-axis parabolic (OAP) mirror with an optical aperture of diameter $D = 50$ mm compatible with this power load will be used for focusing

TABLE I. Characteristics of amplifier modules used in the proposed pulse-burst setup.

	Laser model			
Parameter	Preamplifier 1 PAR HP	Preamplifier 2 PAR HP	Preamplifier 3 PAR LAHP (two sections)	Final amplifier PAR HPHE (two sections)
Active volume (mm^3)	10 × 20 × 800	10 × 20 × 800	22 × 22 × 800 × 2	45 × 45 × 1000 × 2
CO_2: N_2: He (bar)	0.3:0.1:9.6	0.2:0.2:9.6	0.5:0.5:9.0	0.5:0.25:7.25
^{18}O content (%)	43	43	43	47
Discharge voltage (kV)	55	70	160	300
Discharge current (kA)	1.7	3.5	4 × 2	10 × 2
Input energy/pulse (mJ)	0.001	2	1	40
Out. energy/pulse (mJ)	16	1	40	200
Train length (pulses)	1	100	100	100
Out. energy/train (J)	NA	0.1	4	20
Average power (W)	2.4	15	600	3000
Wall-plug power (kW)	5	13	30 × 2	160 × 2

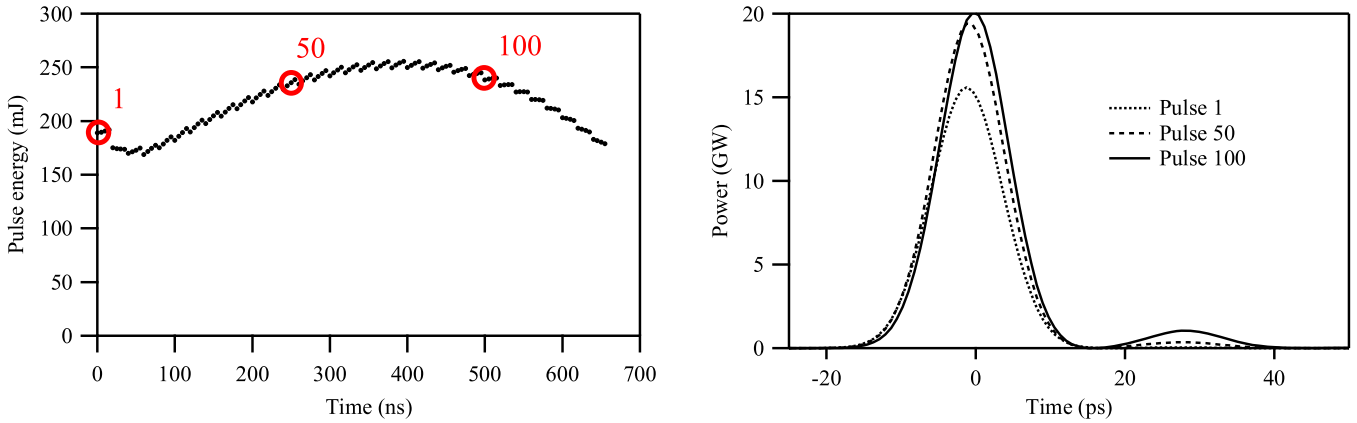

FIG. 2. Simulations for 100-pulse trains with $T_b = 5$ ns and individual pulse duration $\tau_L = 5$ ps (12 ps FWHM). Left: After the final amplifier with marked positions for the first, 50th, and 100th pulses in a train. Right: Temporal envelopes for the first, 50th, and 100th pulses in a train.

the laser beam at the IP. Our beam focusing geometry is chosen according to two ICS examples considered in Sec. IV: The doubled Rayleigh length of the laser focus fits to the electron bunch duration and needs to be 4 mm for 5-ps (rms) bunches and 40 mm for 50-ps bunches. Assuming $M^2 = 1.2$, this defines the corresponding laser focusing to $\sigma_L = \frac{1}{2}\sqrt{\frac{\lambda Z_0 M^2}{\pi}} \approx 40$ μm for 5-ps bunches and $\sigma_L \approx 133$ μm for 50-ps bunches that will require the focus length $F = \frac{\pi D \sigma_L}{M^2 \lambda} = 57$ cm and $F = 170$ cm, correspondingly. A few-millimeter-diameter central hole in the focusing mirror for the e-beam transmission, which proved not to affect the focus quality and has been routinely used in the ATF's ICS experiments [19,20], allows us to put the OAP mirror at the exact counterpropagation geometry to maximize the efficiency of the laser–e-bunch interaction. With the addition of an optional confocal OAP mirror, the laser beam can be recollimated and used at another IP set along the e-beam propagation, thereby multiplying the number of workstations.

IV. PERSPECTIVE ICS SOURCES BASED ON DAΦNE AND CBETA ACCELERATORS

Facing a diversity of potential requirements for future ICS applications, we offer a detailed performance characterization for different examples of perspective ICS sources based on a synchrotron accelerator DAΦNE and an SERL CBETA, each paired either with a near-IR solid-state laser or with an LWIR gas laser. We will show that the LWIR laser (described in the previous section) with its 15 kHz cumulative pulse repetition rate can produce average spectral fluxes and brightness competitive with the proposed earlier multimegahertz solid-state laser-based FEC approach. Simultaneously, this laser driver will provide about 4 orders of magnitude higher x-ray peak characteristics, making such ICS sources interesting for ultrafast applications as well.

A. CBETA

The Cornell-BNL ERL Test Accelerator, or CBETA, is a high-repetition-rate SERL. Table II, column "CBETA," includes the main machine parameters. A recent proposal [5] suggests converting this accelerator into an ICS x-ray source by colliding electron bunches spaced by 0.77 ns with synchronized, mode-locked, Nd:YAG laser pulses circulating inside a Fabry-Perot cavity. Characteristic for linac short electron bunches, $\tau_e = 4$ ps, and their tight focusing to $\sigma_e = 3.2$ μm allows an efficient overlap with $\tau_L = 5.7$ ps laser pulses despite a relatively big collision angle of 18° between the laser and electron beams.

The choice of the drive laser wavelength (1.06 μm) and the electron beam energy (150 MeV) fixes the maximum energy of the ICS x-ray beam at 427 keV [see Eq. (1)], which is above the high-energy cutoff of contemporary SLSs. ERL does not offer the flexibility of a continuously variable e-beam energy. However, the x-ray energy still can be changed stepwise by setting the IP in four arches of the ERL after, correspondingly, the first, second, third, and fourth passes, where discrete electron energies of 42, 78, 114, and 150 MeV, respectively, will be attained. This results in a set of x-ray energies ranging from 427 down to 33.5 keV. A comprehensive set of relevant parameters characterizing this ICS source, calculated using formulas in Sec. III A for the 150 MeV electron beam, is compiled in Table II in the "CBETA-1.06 μm" column.

The predicted high average flux $\mathcal{F}_{av} = 5.8 \times 10^{11}$ ph/s is well suited for high-energy x-ray diffraction, atomic physics, and spectroscopy studies, which require x rays in the 50–150 keV energy range. At the same time, a moderate number of x rays per each shot, $N_\gamma = 10^3$, limits the application of such an ICS source primarily to those measurements where data are accumulated over multiple shots. Examples of such applications are phase contrast imaging, absorption radiography, K-edge subtraction

TABLE II. Parameters of ICS sources based on CBETA and DAΦNE electron accelerators driven by Nd:YAG or CO_2 lasers.

Symbol	Parameter	CBETA		DAΦNE	
λ	Laser wavelength (μm)	1.06	9.2	1.06	9.2
$\mathcal{E}_e$	Beam energy (MeV)	150		510	
γ	Electron gamma factor	300		1000	
$\Delta\mathcal{E}_e/\mathcal{E}_e$	Beam energy spread (rms)	0.05%		0.06%	
T_b	Bunch periodicity (ns)	0.77	3.1	5.4	
f_e	Bunches per sec	1.3 GHz	325 MHz	184 MHz	
τ_e	Bunch rms length (ps)	4		50	
C	Bunch charge (pC)	32	123	8152	
N_e	Electrons per bunch	2×10^8	7.7×10^8	5×10^{10}	
ϵ_n	Beam emittance (mm mrad)	0.3		0.1	
σ_e	Beam radius at IP (μm)	3.2		40×600	
τ_L	Laser pulse rms length (ps)	5.7	5.3	20	42
E_L	Laser pulse energy at IP (mJ)	0.06	200	0.2	200
N_L	Laser photons per pulse	3×10^{14}	9×10^{18}	10^{15}	9×10^{18}
I_L	Laser peak power at IP	10 MW	13 GW	10 MW	1.6 GW
f_L	Laser pulses per sec	1.3×10^9	15×10^3	184×10^6	15×10^3
P_{av}	Laser average power at IP (kW)	81	3	36.8	3
σ_L	Laser rms radius at IP (μm)	25	40	40	133
ϕ	Collision angle	18°	0°	8°	0°
$\mathcal{E}_\gamma$	Gamma energy (MeV)	0.427	0.049	4.94	0.566
τ_γ	Gamma pulse rms length (ps)	4		50	
f_γ	Gamma repetition rate	1.3 GHz	15 kHz	184 MHz	15 kHz
σ_γ	Gamma beam radius at IP (μm)	3.2		40	40×133
N_γ/N_e	Conversion efficiency	2.2×10^{-6}	6×10^{-2}	10^{-7}	5×10^{-4}
N_γ	Gamma per pulse (ph)	450	4.7×10^7	4.8×10^3	2.9×10^7
$\mathcal{F}_{av}$	Average flux (ph/s)	5.8×10^{11}	7.5×10^{11}	9.1×10^{11}	4.3×10^{11}
$\mathcal{F}_p$	Peak flux (ph/s)	4.5×10^{13}	5.3×10^{18}	4.2×10^{13}	2.3×10^{17}
$\mathcal{F}_{0.1\%av}$	Average spectral flux[a]	8.7×10^8	1.1×10^9	1.4×10^9	6.4×10^8
$\mathcal{F}_{0.1\%p}$	Peak spectral flux[a]	6.7×10^{10}	8×10^{15}	6.3×10^{10}	3.4×10^{14}
$\mathcal{B}_{av}$	Average brightness[b]	4.9×10^{13}	6.1×10^{13}	7.4×10^{15}	3.8×10^{15}
$\mathcal{B}_p$	Peak brightness[b]	4.2×10^{15}	4.4×10^{20}	3.4×10^{17}	2.2×10^{21}
$\Delta\mathcal{E}_\gamma/\mathcal{E}_\gamma$	Gamma energy spread (BW)	1.4%		0.85%	
$\mathcal{F}_{av,BW}$	Average flux in BW (ph/s)	9.3×10^9	7.8×10^9	5.5×10^9	1.6×10^{10}
$\mathcal{F}_{p,BW}$	Peak flux in BW (ph/s)	7.6×10^{11}	5.5×10^{16}	2.5×10^{11}	9.0×10^{15}
SPD_{av}	Average spectral density[c]	1.1×10^6	1.2×10^6	7.7×10^4	9.3×10^5
SPD_p	Peak spectral density[c]	9.0×10^7	8.1×10^{13}	3.6×10^6	5.1×10^{11}

[a] $\mathrm{ph}/(\mathrm{s} \cdot 0.1\%BW)$.

[b] $\mathrm{ph}/(\mathrm{s} \cdot \mathrm{mm}^2 \cdot \mathrm{mrad}^2 \cdot 0.1\%BW)$.

[c] $\mathrm{ph}/(\mathrm{s} \cdot \mathrm{eV})$.

imaging, radiotherapy, and computed tomography of stationary samples.

The concept proposed here of using bursts of high peak power CO_2 laser pulses offers a solution for enhancing the peak ICS parameters by several orders of magnitude without losing the average photon flux. The laser parameters for this demonstration are set according to the technology capabilities described in Sec. III. All x-ray calculations for the LWIR laser case were made by averaging over 100 laser pulses from the top of the pulse train.

A 200-mJ LWIR laser pulse focused to $\sigma_L = 40$ μm carries 1.3×10^{36} $\mathrm{ph}/(s \cdot \mathrm{cm}^2)$, which is 10^4 higher compared to the $\lambda = 1.06$ μm FEC example. With a double-Rayleigh-length fitting to the longitudinal span of an electron bunch, we ensure the resulting x-ray scattering efficiency $N_\gamma/N_e = 6\%$ from the laser-electron interaction, which is also over $10^4\times$ compared to the $\lambda = 1.06$ μm FEC example.

The e-beam's normalized emittance is the dominant contribution to the BW at CBETA, resulting in $BW = 1.4\%$ for the 1-μm case. In the LWIR case, the second contribution comes from a relatively short laser pulse that comprises only about 200 laser wavelengths. For a fair comparison with the 1-μm case, we bring the total BW parameter to the same 1.4% level by restricting the acceptance angle Ψ (see Table III).

We note that CBETA allows two different modes of operation with 1.3 GHz and 325 MHz bunch repetition

TABLE III. Individual contributions to BW for ICS sources in Table II.

	Accelerator Laser λ			
	CBETA		DAΦNE	
Contribution	1.06 μm	9.2 μm	1.06 μm	9.2 μm
Electron emittance	1%		0.5%	
Electron energy spread	0.1%		0.12%	
Laser band	<0.1%	0.3%	<0.1%	
Laser diffraction	<0.1%	<0.1%	<0.1%	
Laser strength	<0.1%	0.2%	<0.1%	
Above combined	1%	1.07%	0.6%	
Acceptance	1%	0.9%	0.6%	
Total BW	1.4%	1.4%	0.85%	

rates. While the first mode fits the 1-μm laser regime considered in the proposal [5], we choose here the lower repetition rate regime that provides 4 times higher electron bunch charges, adding to the higher x-ray yield, which will now reach 4.7×10^7 ph/pulse to surpass by 10^5 times the corresponding number for the 1.06-μm case. The peak flux and brightness of the 49-keV ICS source driven by the 9.2-μm lasers also exceed those for the 1.06-μm case by the same factor, making the CBETA ICS source highly potent for dynamic pump-probe-type applications.

At the same time, a still substantial 15 kHz cumulative repetition rate of $\lambda = 9.2$ μm laser pulses allows us to reach high average x-ray yield parameters identical to a multimegahertz FEC-based ICS source. This makes the LWIR-based source equally useful for studies intended for the 1.06-μm-based source but surely in a different spectral range closer to conventional SLSs. Its x-ray coverage, corresponding to first, second, third, and fourth passes in the ERL beam arches, will span from 4 up to 49 keV.

B. DAΦNE

The approach presented above to an ICS based on LWIR pulse trains is not unique for CBETA but can be adapted to a variety of accelerators. We consider here another example: a synchrotron damping ring, which has a different bunch format. DAΦNE (Double Annual Φ-factory for Nice Experiments) is an e^+e^- collider at INFN Frascati, operating at 510 MeV energy in each beam. Other main machine parameters can be found in Table II in the column "DAΦNE." We will show that a CO_2 laser configuration similar to the one considered for the CBETA ERL can be utilized to reach superior peak parameters for the DAΦNE storage ring compared to the 1.06-μm FEC approach elaborated in a proposal [6]. The Nd:YAG laser parameters assumed in that proposal are similar to those of the FEC designed and fabricated at LAL Orsay and used in the KEK experiment [17]. Laser pulses within the IP are synchronized with electron bunches spaced by 5.4 ns. A collision angle between the laser and electron beams is set at 8°, and the repetition frequency of collisions is 184 MHz. In view of a big disparity in the e-beam's horizontal and vertical sizes, which is characteristic of synchrotron storage rings, symmetrization of the e-beam divergence at the IP required setting the ratio between beta functions in both the vertical and horizontal planes equal to the machine coupling, $\beta_x/\beta_y = 15$. This defines a flat 40×600 μm cross section of the e-beam at IP. In spite of the fact that a 1.06-μm laser with the 40 μm beam cross section can interact only with a small portion (~6%) of such a flat e-beam, an extremely high current stored in the electron ring still allows one to achieve gamma-ray fluxes close to $\mathcal{F}_{av} \approx 10^{12}$ ph/s. In addition, an excellent e-beam emittance $\epsilon_n = 0.1$ mm mrad defines a high average brightness $B_{av} \approx 7 \times 10^{15}$ ph/(s · mm^2 · mrad^2 · 0.1%BW). The total spectral bandwidth $BW \approx 0.85\%$ is primarily emittance limited and results in a high monochromaticity of the proposed gamma source. The x-ray flux and spectral density into this BW can be found in Table II as well.

At the same time, the peak flux and brightness of this FEC-based source are just 45 times above their average values, which is not surprising considering that the produced gamma photons are contained in 50-ps rms pulses at the 184 MHz repetition rate, resulting in a duty factor $2\sqrt{2\ln 2}\tau_\gamma \times f_\gamma = 0.022$. Similar to the above CBETA example, such a FEC-based ICS source can be applied primarily to quasistatic measurements where the process data are accumulated over multiple shots.

A comprehensive set of relevant parameters characterizing this ICS source compiled from Ref. [6] and calculated using formulas in Sec. II A is presented in Table II in the column "DAΦNE – 1.06 μm" for a core electron energy of 510 MeV, resulting in the gamma energy 4.94 MeV. It has been suggested that varying the e-beam energy might produce extreme gamma-ray beams between 9 and 2 MeV, which are desirable for nuclear physics and nuclear photonics experiments.

It has been also noted that using a CO_2 laser may allow one to expand the spectral coverage down to 200 keV. The authors of Ref. [6] further argued that "However, in this latter case, because of the available technology, lower laser power will be available and, as a consequence, reduced gamma fluxes can be obtained." Our proposed concept of using bursts of CO_2 laser pulses offers a solution for boosting the ICS peak parameters by several orders of magnitude without losing the average photon flux. Simultaneously, the spectral coverage moves from the gamma range into the 200–900 keV hard x-ray range.

A relatively long, 50-ps rms bunch length explains the choice of a 50-ps laser pulse for this demonstration, which can be obtained from the laser system described in Sec. III. To allow for efficient interaction between electron bunches and laser pulses over their entire temporal overlap, the Rayleigh length of the laser focus should be extended accordingly. Focused to $\sigma_L = 133$ μm, the $\lambda = 9.2$ μm

beam allows an efficient energy exchange with electrons, subject to limitations due to the flat e-beam profile. We see in Table II that the expanded laser pulse does not contribute to the bandwidth, which is still defined primarily by the electron beam emittance and is of the same value quoted for the DAΦNE – 1.06 μm case.

The calculated parameters for the proposed CO_2 laser-driven ICS source of the 566 keV gamma rays are compiled in Table II in the column "DAΦNE – 9.2 μm." The attained number of $\sim 3 \times 10^7$ photons/pulse is close to the CBETA example. Combined with the extremely high peak brightness $B_p \approx 2 \times 10^{21}$ ph/$(s \cdot mm^2 \cdot mrad^2 \cdot 0.1\%BW)$, the proposed source will be indispensable for dynamic studies in the hard x-ray range that are not covered by conventional SLSs.

V. SUMMARY AND CONCLUSIONS

In this paper, we introduced a concept of using bursts of LWIR laser pulses for building high peak brightness ICS sources based on existing rf electron accelerators. To realize this concept, we proposed a new architecture of LWIR laser based on available and emerging CO_2 gas laser technology. As examples, we elaborated here on ICS source design parameters of the DAΦNE and CBETA electron accelerators, which have been considered for conversion into x-ray and gamma-ray user facilities.

In addition to the typical applications attained with third-generation SLSs, the CBETA ICS source can be used for time-resolved studies where high-repetition machines are difficult to fit. These applications, more typical for fourth-generation coherent SLSs, include dynamic molecular reaction microscopes, time-resolved photoemission and absorption spectroscopy, time-resolved resonant inelastic x-ray scattering, x-ray photon correlation spectroscopy, time-resolved x-ray scattering, and pump-probe experiments.

The x-ray brightness is usually the main parameter used to characterize and compare different light sources. Therefore, it is instructive to compare existing and emerging light sources by this parameter, as we do in Fig. 3.

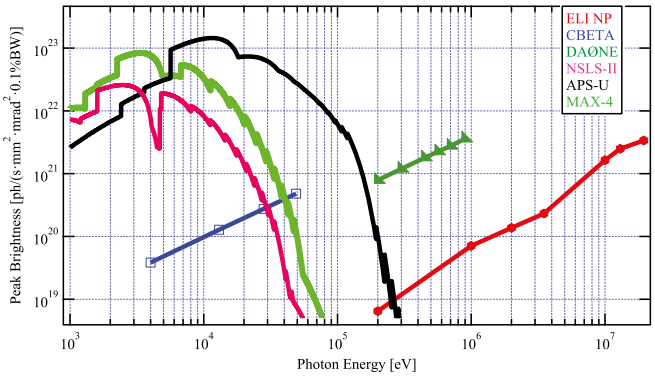

FIG. 3. Positioning ICS sources CBETA-9 mm and DAΦNE-9 mm in terms of their peak brightness in comparison with third-generation SLSs and ELI-NP.

One can see that the relatively compact CBETA ICS source proposed here, which is ~100 times smaller in footprint compared to existing or under-construction third-generation SLSs, can be considered a viable complement, especially at the high-energy end. Hard x-ray pulses at 20–50 keV from a CBETA ICS source will help to reveal ultrafast structural dynamics in a wide range of molecules, allowing us to explore their structural changes immediately upon optical excitation.

Additive manufacturing is another area where x-ray imaging can make a substantial impact. It is a suite of powerful techniques focused on the production of highly reliable engineering devices, such as the active elements of biomedical machines, turbine parts, and battery elements. In particular, laser additive manufacturing [21] includes laser powder fusion and direct-energy deposition and is a widely used process for fusing metallic, ceramic, or other powders for constructing complex 3D shapes. The manufacturing processes require sensitive x-ray diagnostics at 20–50 keV that search for microscale violations of the parts' accuracy, hidden structural defects, loss of bonding, voids, and contamination.

In addition to having the advantage of a compact footprint, a characteristic it shares with CBETA, the projected DAΦNE ICS source will offer extended spectral coverage into the gamma range, up to 900 keV, where it can be compared in the peak brightness and repetition rate only to the ELI-NP facility. Similar to ELI-NP, which is currently under construction, with the proposed DAΦNE ICS, researchers will be able to investigate fundamental problems and applications in the field of nuclear physics, such as the study of photonuclear processes using tunable energy, high-resolution γ-ray beams.

Overall, the desired ability to deliver x-ray and gamma-ray radiation is case specific with the required energy coverage spanning several decades, which cannot be satisfied by a single source. Therefore, a variety of different kinds of ICS sources based on the combined capabilities of ring-based and linac-based sources, as well as different laser drivers, will be needed to provide a sufficiently broad range of characteristics required to meet current user requirements and future challenges.

ACKNOWLEDGMENTS

The authors thank Dr. David Alesini (Instituto Nazionale di Fisica Nucleare) and Dr. Dejan Trbojevic (BNL) for helpful discussions. This work is funded by the U.S. Department of Energy under Contract No. DE-SC0012704.

[1] G. Krafft and G. Priebe, Compton sources of electromagnetic radiation, Rev. Accel. Sci. Techol. **03**, 147 (2010).
[2] The Lyncean Compact Light Source, White paper, https://lynceantech.com/marketing/downloads/Lyncean_CLS_Whitepaper_Stepping-stone_to_Synchrotron.pdf.

[3] T. Akagi *et al.*, Narrow-band photon beam via laser Compton scattering in an energy recovery linac, Phys. Rev. Accel. Beams **19**, 114701 (2016).
[4] ELI-NP White Book, http://www.eli-np.ro/documents/ELI-NP-WhiteBook.
[5] K. E. Deitrick *et al.*, A hard x-ray compact Compton source at CBETA, in *Proceedings of IPAC2019, Melbourne, Australia* (JACoW, Geneva, 2019), https://doi.org/10.18429/JACoW-IPAC2019-TUPGW085.
[6] D. Alesini, I. Chaikovska, S. Guiducci, C. Milardi, A. Variola, M. Zobov, and F. Zomer, DAΦNE γ-rays factory, IEEE Trans. Nucl. Sci. **63**, 913 (2016).
[7] Z. Huang and R. D. Ruth, Laser-Electron Storage Ring, Phys. Rev. Lett. **80**, 976 (1998).
[8] O. R. Wood, R. L. Abrams, and T. J. Bridges, Mode locking of a transversely excited atmospheric pressure CO_2 laser, Appl. Phys. Lett. **17**, 376 (1970).
[9] P. B. Corkum and C. Roland, High energy picosecond 10 μm pulses, Proc. SPIE Int. Soc. Opt. Eng. **664**, 212 (1986).
[10] H. von Bergmann, High pressure CO_2 amplifiers for picosecond pulse amplification, Proc. SPIE Int. Soc. Opt. Eng. **11042**, 110420N (2019).
[11] F. Morkel, PAR Systems (private communication).
[12] V. Petrillo *et al.*, Photon flux and spectrum of gamma-ray sources, Nucl. Instrum. Methods Phys. Res., Sect. A **693**, 109 (2012).
[13] M. N. Polyanskiy, I. V. Pogorelsky, M. Babzien, and M. A. Palmer, Demonstration of a 2 ps, 5 TW peak power, long-wave infrared laser based on chirped-pulse amplification with mixed-isotope CO_2 amplifiers, OSA Continuum **3**, 459 (2020).
[14] I. V. Pogorelsky, J. Fischer, K. P. Kusche, M. Babzien, N. A. Kurnit, I. J. Bigio, R. F. Harrison, and T. Shimada, Subnanosecond multi-gigawatt CO_2 laser, IEEE J. Quantum Electron. **31**, 556 (1995).
[15] M. N. Polyanskiy and M. Babzien, Ultrashort pulses, in *CO_2 Laser—Optimization and Application*, edited by D. C. Dumitras (National Institute for Laser Plasma and Radiation Physics, Romania, 2012), p. 139, https://doi.org/10.5772/37648.
[16] M. N. Polyanskiy, I. V. Pogorelsky, and V. Yakimenko, Picosecond pulse amplification in isotopic CO_2 active medium, Opt. Express **19**, 7717 (2011).
[17] M. N. Polyanskiy, CO2AMP: A software program for modeling the dynamics of ultrashort pulses in optical systems with CO_2 amplifiers, Appl. Opt. **54**, 5136 (2015).
[18] M. N. Polyanskiy, M. Babzien, and I. V. Pogorelsky, Chirped-pulse amplification in a CO_2 laser, Optica **2**, 675 (2015).
[19] M. Babzien, I. Ben-Zvi, K. Kusche, I. V. Pavlishin, I. V. Pogorelsky, D. P. Siddons, V. Yakimenko, D. Cline, F. Zhou, T. Hirose, Y. Kamiya, T. Kumita, T. Omori, J. Urakawa, and K. Yokoya, Observation of the Second Harmonic in Thomson Scattering from Relativistic Electrons, Phys. Rev. Lett. **96**, 054802 (2006).
[20] A. Ovodenko, R. Agustsson, M. Babzien, T. Campese, M. Fedurin, A. Murokh, I. Pogorelsky, M. Polyanskiy, J. Rosenzweig, Y. Sakai, T. Shaftan, and C. Swinson, High duty cycle inverse Compton scattering x-ray source, Appl. Phys. Lett. **109**, 253504 (2016).
[21] C. Lun, A. Leung, S. Marussi, R. C. Atwood, M. Towrie, P. J. Withers, and P. D. Lee, In situ x-ray imaging of defect and molten pool dynamics in laser additive manufacturing, Nat. Commun. **9**, 1355 (2018).